Effect of *tert*-butyl substitution on controlling the orientation of TADF emitters in guest-host systems

Prakhar Sahay[1], Ettore Crovini[2], Kleitos Stavrou[3], Zhen Zhang[4], Bình Minh Nguyễn[1], Daniel Wagner[5], Peter Strohriegl[5], Stefan Bräse[4,6], Andrew Monkman[3], Eli Zysman-Colman[2]*, Wolfgang Brütting[1]*

[1] Experimental Physics IV, Institute of Physics, University of Augsburg, Augsburg, Germany.

[2] Organic Semiconductor Centre, EaStCHEM School of Chemistry, University of St Andrews, St Andrews, United Kingdom.

[3] Department of Physics, Durham University, Stockton Road, Durham, United Kingdom

[4] Institute of Organic Chemistry, Karlsruhe Institute of Technology, Karlsruhe, Germany

[5] Macromolecular Chemistry, University of Bayreuth, Bayreuth, Germany

[6] Institute of Biological and Chemical Systems – Functional Molecular Systems, Karlsruhe Institute of Technology, Eggenstein-Leopoldshafen, Germany

* Corresponding Authors:
Prof. Wolfgang Brütting, wolfgang.bruetting@uni-a.de
Prof. Eli Zysman-Colman, eli.zysman-colman@st-andrews.ac.uk

SUPPORTING INFORMATION

General Methods **S2**

Synthesis **S4**

DFT Calculations **S9**

Thermal analysis **S13**

Molecular geometry, thickness, and aspect ratio effect **S16**

Orientation Measurements **S18**

OLED Device Data **S20**

Light Outcoupling Simulation **S21**

References **S22**

General Methods

General Characterization

NMR spectra were recorded using the following instrument: ^{1}H NMR: *Bruker* Avance 400 (400 MHz). Chloroform-d_1 from *Eurisotop* was used. Chemical shifts δ were expressed in parts per million (ppm) and referenced to chloroform (^{1}H: δ = 7.26 ppm). All coupling constants are absolute values and expressed in Hertz (Hz). Electron Spray Ionization (ESI) experiments were recorded on a Q-Exactive (Orbitrap) mass spectrometer (Thermo Fisher Scientific, San Jose, CA, USA) equipped with a HESI II probe to record high resolution. The infrared spectra of solid samples were recorded on Bruker IFS 88 and measured by attenuated total reflection (ATR method). Absorption is given in wavenumbers $\bar{\upsilon}$ [cm^{-1}]. Analytical thin-layer chromatography (TLC) was carried out on Merck silica gel coated aluminium plates (silica gel 60, F254), detected under UV-light at 254 nm. Solvents, reagents, and chemicals were purchased from Sigma-Aldrich, Chempure, ABCR and Acros Organics. All solvents, reagents and chemicals were used as purchased unless stated otherwise.

Time-Resolved Photoluminescence Measurements

Time-resolved measurements were performed using a spectrograph (Horiba Triax) and a Stanford Computer Optics 4 Picos intensified charge-coupled device camera, where samples were excited with a Nd:YAG laser (EKSPLA, 10 Hz, 355 nm), under vacuum.

Angular Dependent Photoluminescence Spectroscopy

The films of the emitters were co-evaporated with different host materials under high vacuum on fused silica substrates. The substrates were then mounted on a rotating stage using index matching gel and irradiated with a UV LED (λ=365 nm) at a vertical irradiance angle of 0° with respect to the substrate normal. The photoluminescence was recorded in s and p polarization mode using 'Phelos' from Fluxim [1, 2] by rotating the sample between -90° and +90° in front of a fiber optical spectrometer. The obtained angular dependent photoluminescence sweeps for both polarizations were simultaneously fitted to calculate the orientation parameter Θ and the film thickness, as well as the intrinsic emission spectrum of the corresponding emitter. The only required input for the fitting were the optical data of the used hosts (refractive index and extinction coefficient between 400 and 800 nm), which were obtained independently from variable angle spectroscopic ellipsometry, including possible birefringence of the films. Further information regarding the method can be found in the references [3, 4].

OLED Devices and Characterization

OLED devices were fabricated on pre-patterned, 90 nm thick Indium Tin Oxide (ITO) layers on glass substrates. These substrates were coated with ~30 nm thick PEDOT:PSS (CLEVIOS P VP AI 4083 from Heraeus). All the organic materials were commercially obtained from Lumtec and deposited under high vacuum (10^{-7} mbar). The OLEDs were then measured using a source meter (Keithley 2400) and a calibrated Si photodiode with a photometric filter (Gigahertz Optik) under N_2 environment inside a glovebox. OLED light outcoupling simulations were carried out using commercially available software 'SETFOS' from Fluxim [5, 6].

Density Functional Theory

Calculations were submitted and processed using the Silico v 0.20.5 software package [7] which incorporates a number of publicly available software libraries, including: cclib [8] for parsing of result files, VMD/Tachyon [9, 10] for 3D rendering, Open Babel/Pybel [11, 12] for file interconversion.

All ground-state optimizations have been carried out using density functional theory (DFT) level implemented within Gaussian [13] in the gas phase, using the PBE0 [14] functional and the 6-31G(d,p) basis set [15]. Excited-state calculations were performed using TD-DFT within the Tamm-Dancoff approximation [16] using the same functional and basis set as for ground-state geometry optimization. This methodology has been demonstrated to show a quantitative estimate of ΔE_{ST} in comparison to experiment [17].

Thermal Analysis

Differential scanning calorimetry (DSC) was performed with a Mettler DSC3+ under nitrogen flow using in pierced Al pans. The glass transition temperature (T_g) was determined as the inflection point of the step in the second heating scan at 10 K/min). T_g has been reported to contribute towards controlling the orientation of the emitter in host materials in literature [18]. Every compound has been subjected to 4 different rates of heating (10 K/min, 10 K/min, 20 K/min and 40 K/min) and 100 K/min cooling cycles to induce amorphous state of the compounds thus insuring reproducibility of the data.

Synthesis

The synthesis of the emitter molecules has been described in this section. [19]

5,11-bis(4-(4,6-bis(4-(tert-butyl)phenyl)-1,3,5-triazin-2-yl)phenyl)-5,11-dihydroindolo[3,2-b]carbazole (ICzTRZ):

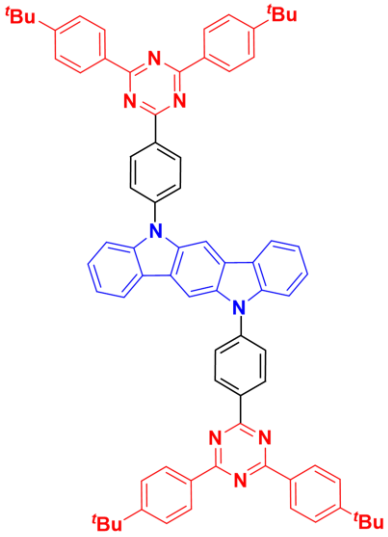

A 50 mL vial was charged with **5,11-Ddihydroindolo[3,2-b]carbazole** (250 mg, 975 μmol, 1.00 equiv.), **2,4-bis(4-(*tert*-butyl)phenyl)-6-(4-fluorophenyl)-1,3,5-triazine** (900 mg, 2.05 mmol, 2.10 equiv.) and tripotassium phosphate (2.07 g, 9.75 mmol, 10.00 equiv.). The vial was sealed, then evacuated and flushed with argon three times. Anhydrous methyl sulfoxide (20 mL) was added through the septum, then the vial was heated to 120 °C and stirred at that temperature for 12 h, before cooling to room temperature. The reaction mixture was diluted with dichloromethane (50 mL) and washed with brine (3 × 50 mL). The organic layer was dried over $MgSO_4$ and the solvent was removed under reduced pressure. The crude product was purified by column chromatography on silica gel (cyclohexane/ dichloromethane = 10/1 to 5/1), providing 0.70 g of target compound.

Yield 66%. **R_f** =0.30 (cyclohexane/dichloromethane = 5:1). **Mp:** 346–348 °C. **^{1}H NMR (400 MHz, $CDCl_3$) δ (ppm)** = 9.09 (d, J = 8.5 Hz, 4H), 8.76 (d, J = 8.5 Hz, 8H), 8.25 (s, 2H), 8.18 (d, J = 7.8 Hz, 2H), 7.95 (d, J = 8.5 Hz, 4H), 7.65 (d, J = 8.6 Hz, 8H), 7.61 (d, J = 8.2 Hz, 2H), 7.47 (t, J = 8.1 Hz, 2H), 7.31 (t, J = 7.4 Hz, 2H), 1.44 (s, 36H). **^{13}C NMR (100 MHz, $CDCl_3$) δ (ppm)** = 171.8 (C_q, 4C_{Ar}), 170.9 (C_q, 2C_{Ar}), 156.3 (C_q, 4C_{Ar}), 142.2 (C_q, 2C_{Ar}), 141.7 (C_q, 2C_{Ar}), 136.9 (C_q, 2C_{Ar}), 135.2 (C_q, 2C_{Ar}), 133.7 (C_q, 4C_{Ar}), 130.9 (+, 4C_{Ar}H), 129.0 (+, 8C_{Ar}H), 126.9 (+, 4C_{Ar}H), 126.5 (+, 2C_{Ar}H), 125.8 (+, 8C_{Ar}H), 124.1 (C_q, 2C_{Ar}), 124.0 (C_q, 2C_{Ar}), 120.6 (+, 2C_{Ar}H), 120.1 (+, 2C_{Ar}H), 109.9 (+, 2C_{Ar}H), 100.4 (+, 2C_{Ar}H), 35.3 (C_q, 4*C*(CH_3)$_3$), 31.4

(+, 12CH_3). **IR** (ATR, $\tilde{\nu}$) = 2958 (w), 1604 (w), 1578 (m), 1504 (vs), 1477 (s), 1460 (m), 1441 (vs), 1408 (s), 1366 (vs), 1324 (m), 1303 (m), 1266 (w), 1234 (m), 1190 (m), 1169 (w), 1149 (w), 1106 (w), 1016 (w), 847 (w), 815 (vs), 758 (w), 738 (s), 701 (w), 565 (m), 550 (m) cm^{-1}. **HRMS** (ESI, $C_{76}H_{70}N_8$) calc. 1094.5723 $[M]^+$, found 1094.5715 $[M]^+$. NMR Spectra of ICzTRZ were shown in reference [19].

5,11-bis(4-(4,6-diphenyl-1,3,5-triazin-2-yl)phenyl)-5,11-dihydroindolo[3,2-b]carbazole (ICzTRZ-0):

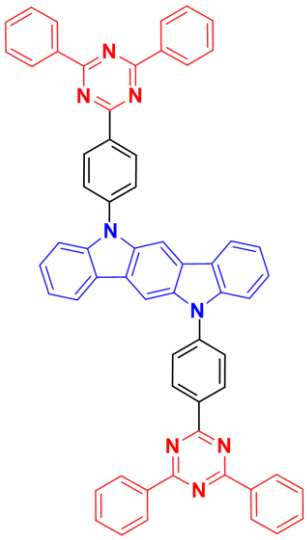

A 50 mL sealed vial was charged with 5,11-dihydroindolo[3,2-b]carbazole (192 mg, 749 µmol, 1.00 equiv.), 2-(4-fluorophenyl)-4,6-diphenyl-1,3,5-triazine (515 mg, 1.57 mmol, 2.10 equiv.) and potassium phosphate tribasic (1.59 g, 7.50 mmol, 10.00 equiv.). It was evacuated and flushed with argon three times. Through the septum 20 mL of anhydrous DMSO were added, then it was heated to 120 °C and stirred for 12 h. After cooling to room temperature, 100 mL water was added to the mixture. Then it was filtered and the solid was thoroughly washed with methanol and dichloromethane to yield a luminescent yellow solid (520 mg, 597 µmol, 80%).

NMR measurements were not successful due to too low solubility. – **IR** (ATR, $\tilde{\nu}$) = 2921 (w), 2853 (w), 1738 (w), 1599 (m), 1588 (m), 1572 (w), 1510 (vs), 1475 (s), 1439 (vs), 1412 (s), 1361 (vs), 1317 (vs), 1303 (s), 1293 (s), 1228 (s), 1198 (m), 1190 (m), 1173 (s), 1164 (s), 1142 (s), 1106 (m), 1064 (m), 1027 (m), 1014 (m), 1000 (w), 969 (w), 952 (w), 929 (m), 851 (w), 840 (w), 829 (s), 819 (w), 766 (vs), 755 (w), 737 (s), 722 (vs), 686 (vs), 676 (s), 662 (m), 645 (m), 637 (m), 629 (w), 564 (s), 509 (m), 466 (w), 408 (w) cm^{-1}. – **HRMS** (ESI) calc. for $C_{60}H_{38}N_8$ $[M]^+$ 870.3219, found 870.3213.

2,8-di-tert-butyl-5,11-bis(4-(4,6-diphenyl-1,3,5-triazin-2-yl)phenyl)-5,11-dihydroindolo[3,2-b]carbazole (d^{t}Bu-ICzTRZ-0):

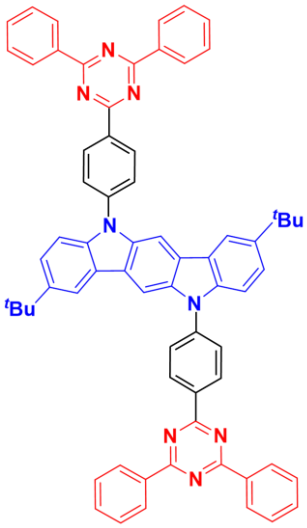

A 50 mL sealed vial was charged with 2,8-di-*tert*-butyl-5,11-dihydroindolo[3,2-b]carbazole (184 mg, 500 µmol, 1.00 equiv.), 2-(4-fluorophenyl)-4,6-diphenyl-1,3,5-triazine (343 mg, 1.05 mmol, 2.10 equiv.) and potassium phosphate tribasic (1.06 g, 5.00 mmol, 10.00 equiv.). It was evacuated and flushed with argon three times. Through the septum 20 mL anhydrous methyl sulfoxide was added, then it was heated to 120 °C and stirred for 12 h. After cooling to room temperature, 100 mL water was added to the mixture. Then it was filtered and the solid was thoroughly washed with methanol and dichloromethane, which yielded the title compound as a luminescent yellow solid (363 mg, 369 µmol, 74%).

R_f = 0.30 (cyclohexane/dichloromethane = 3:1). – **^{1}H NMR** (400 MHz, $CDCl_3$) δ = 9.12 (d, *J* = 8.4 Hz, 4H), 8.87 (dd, *J* = 8.0 Hz, *J* = 1.8 Hz, 8H), 8.26 (s, 2H), 8.19 (s, 2H), 7.99 (d, *J* = 8.5 Hz, 4H), 7.76–7.60 (m, 12H), 7.59–7.51 (m, 4H), 1.47 (s, 18H) ppm. – **^{13}C NMR** measurements were not successful due to too low solubility. – **IR** (ATR, ṽ) = 2963 (w), 2949 (w), 1602 (w), 1588 (w), 1514 (vs), 1482 (m), 1455 (s), 1443 (s), 1412 (w), 1366 (vs), 1322 (m), 1283 (m), 1256 (w), 1234 (w), 1224 (w), 1201 (w), 1171 (m), 1146 (m), 1133 (w), 1026 (w), 1016 (w), 847 (w), 830 (m), 809 (w), 773 (m), 758 (m), 735 (m), 690 (vs), 679 (w), 656 (w), 646 (m), 618 (w), 588 (m), 571 (w), 507 (w), 466 (w), 409 (w) cm^{-1}. – **HRMS** (ESI) calc. for $C_{68}H_{54}N_8$ $[M]^+$ 982.4471, found 982.4479.

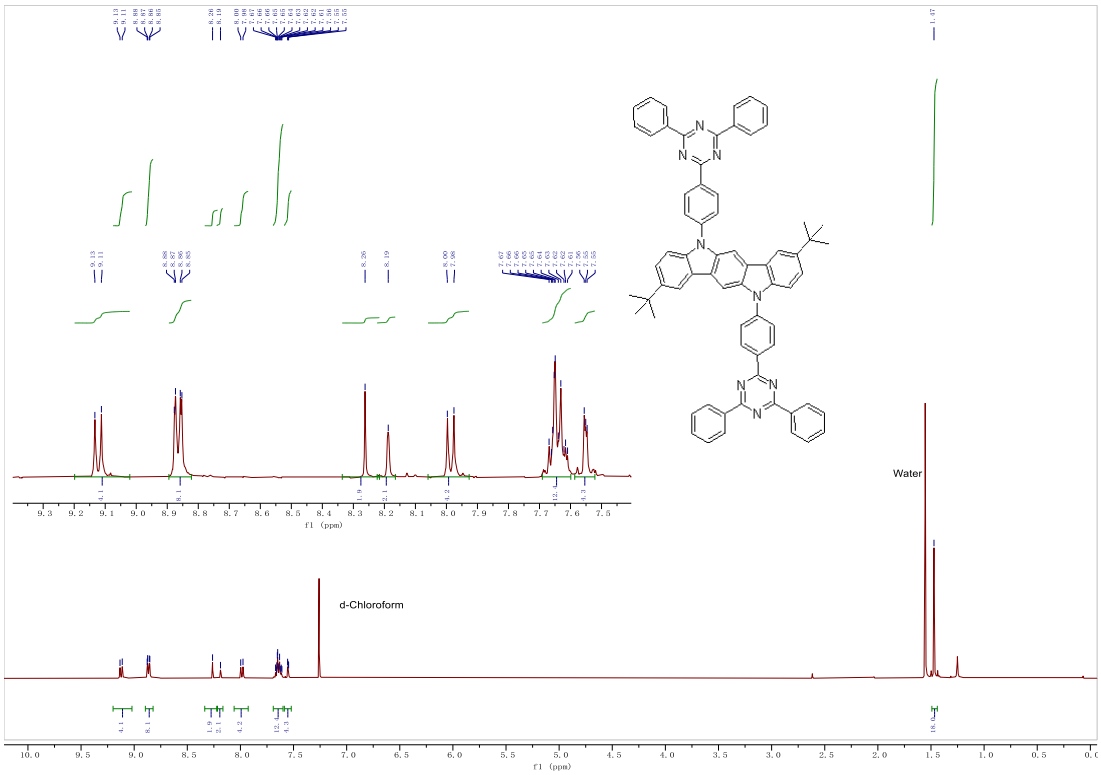

Figure S1. ^{1}H NMR of **d^{t}Bu-ICzTRZ-0** in $CDCl_3$.

5,11-bis(4-(4,6-bis(4-(tert-butyl)phenyl)-1,3,5-triazin-2-yl)phenyl)-2,8-di-tert-butyl-5,11-dihydroindolo[3,2-b]carbazole (d^{t}Bu-ICzTRZ):

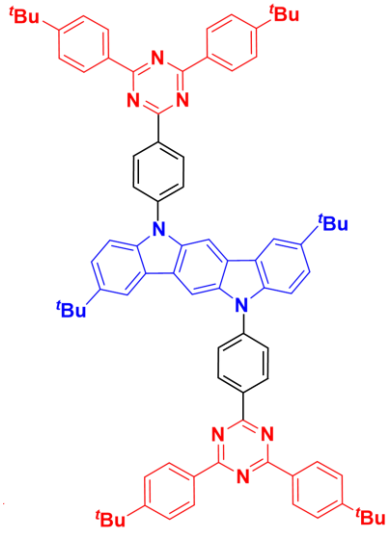

A 50 mL sealed vial was charged with 2,8-di-*tert*-butyl-5,11-dihydroindolo[3,2-b]carbazole (125 mg, 339 μmol, 1.00 equiv.), 2-(4-fluorophenyl)-4,6-diphenyl-1,3,5-triazine (372 mg, 846 μmol, 2.50 equiv.) and potassium phosphate tribasic (0.72 g, 3.39 mmol, 10.00 equiv.). It was evacuated and flushed with argon three times. Through the septum 20 mL anhydrous methyl sulfoxide was added, then it was heated to 120 °C and stirred for 12 h. After cooling to room

temperature, the reaction mixture was diluted with dichloromethane (200 mL) and washed with brine (3 × 50 mL). The organic layer was dried over $MgSO_4$ and the solvent was removed under reduced pressure. The crude product was purified by column chromatography on silica gel (cyclohexane/ dichloromethane = 10:1 to 6:1) to yield the title compound as a yellow luminescent solid (300 mg, 248 µmol, 73%).

R_f = 0.40 (cyclohexane/dichloromethane = 5:1). – **^{1}H NMR** (400 MHz, $CDCl_3$) δ = 9.10 (d, *J* = 8.5 Hz, 4H), 8.76 (d, *J* = 8.5 Hz, 8H), 8.26 (s, 2H), 8.19 (s, 2H), 7.97 (d, J = 8.4 Hz, 4H), 7.64 (d, J = 8.5 Hz, 8H), 7.55 (s, 4H), 1.54 (s, 18H), 1.47 (s, 18H) ppm. – **^{13}C NMR** measurements were not successful due to too low solubility. – **IR** (ATR, ṽ) = 2962 (w), 1604 (w), 1578 (w), 1503 (vs), 1455 (vs), 1409 (m), 1367 (vs), 1356 (vs), 1322 (m), 1288 (w), 1264 (m), 1235 (w), 1201 (w), 1190 (m), 1170 (m), 1149 (w), 1106 (w), 1017 (w), 868 (w), 851 (m), 836 (w), 819 (vs), 809 (s), 738 (m), 718 (w), 705 (w), 589 (m), 571 (w), 551 (s), 504 (w), 415 (w) cm^{-1}. – **HRMS** (ESI) calc. for $C_{84}H_{86}N_8$ $[M]^+$ 1206.6975, found 1206.6991.

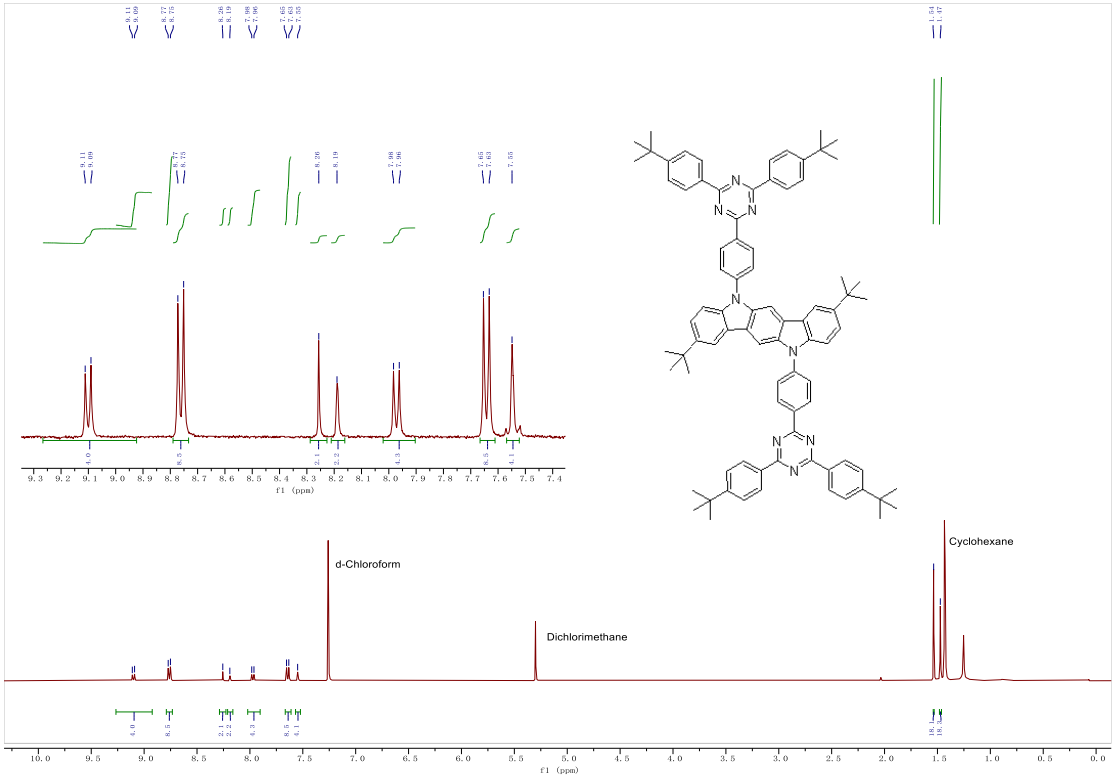

Figure S2. ^{1}H NMR of **d^{t}Bu-ICzTRZ** in $CDCl_3$.

DFT Calculations

Table S1. Excited states properties of **ICzTRZ**

Excited State	**Energy (eV)**	**Nature**	**Character of the transition**
T_1	2.70	HOMO-2→LUMO+1 (5%) **HOMO→LUMO (82%)** HOMO→LUMO+10 (5%)	CT
T_2	2.75	HOMO-2→LUMO (7%) **HOMO→LUMO+1 (82%)** HOMO→LUMO+6 (3%)	CT
T_3	2.83	**HOMO → LUMO+4 (90%)**	LE (ICz)
S1 (f=0.72)	2.92	**HOMO → LUMO (98%)**	CT

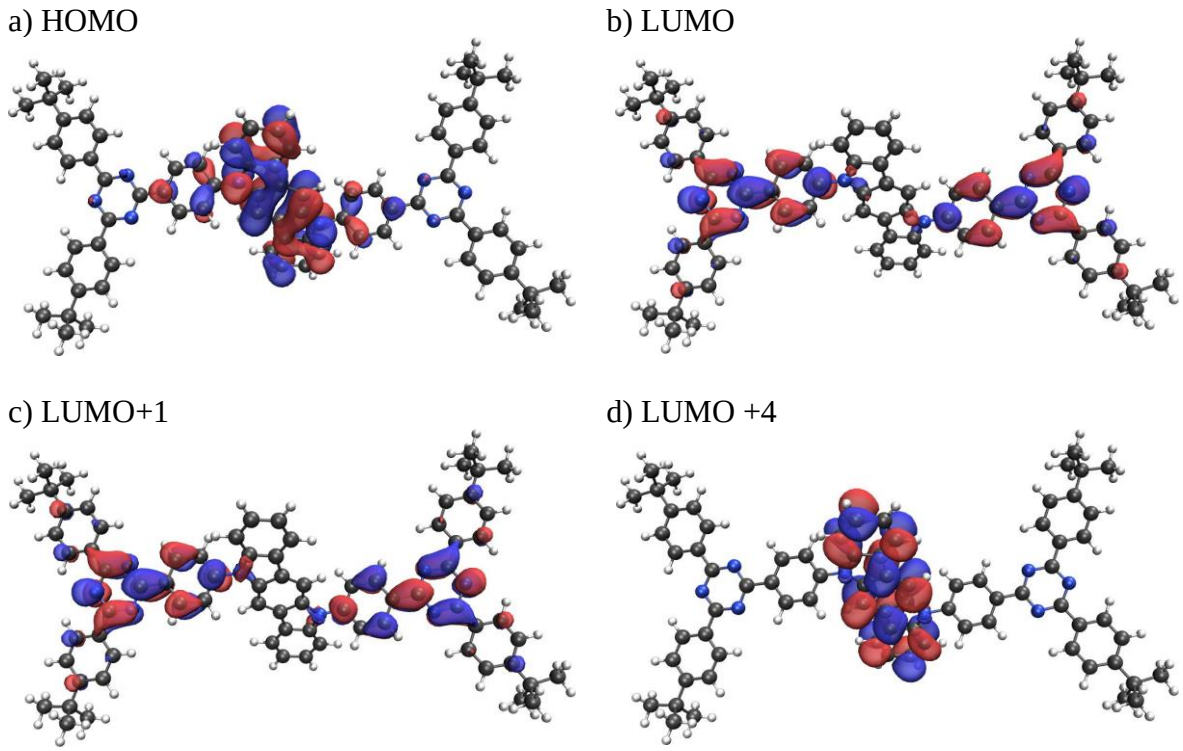

Figure S3. Electronic density surfaces of **ICzTRZ.** a) HOMO, b) LUMO, c) LUMO+1, d) LUMO +4 (Isovalue for new surfaces: MO=0.02, Density=0.0004).

Table S2. Excited-state properties of **ICzTRZ-0**.

Excited State	**Energy (eV)**	**Nature**	**Character of the transition**
T_1	2.67	HOMO-2→LUMO+1 (5%) **HOMO→LUMO (84%)** HOMO→LUMO+5 (3%)	CT
T_2	2.70	HOMO-2→LUMO (6%) **HOMO→LUMO+1 (83%)** HOMO→LUMO+6 (2%)	CT
T_3	2.83	**HOMO → LUMO+4 (91%)**	LE (ICz)
S1 (f=0.68)	2.88	**HOMO → LUMO (97%)**	CT

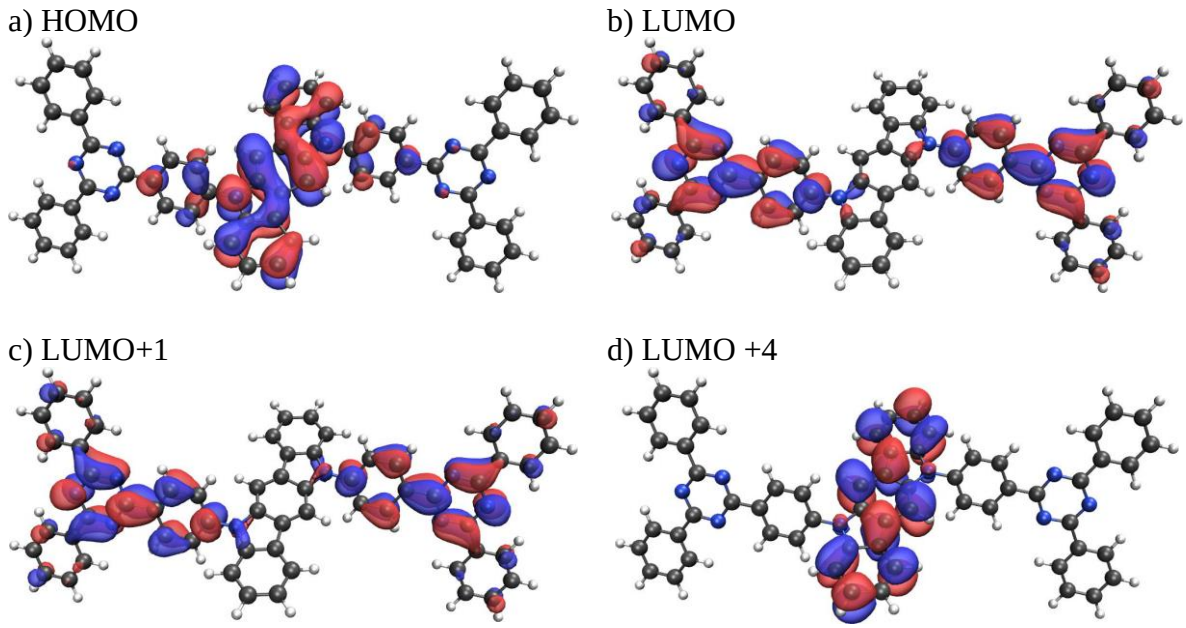

Figure S4. Electronic density surfaces of **ICzTRZ-0**. a) HOMO, b) LUMO, c) LUMO+1, d) LUMO +4 (Isovalue for new surfaces: MO=0.02, Density=0.0004).

Table S3. Excited states properties of **d^{t}Bu-ICzTRZ-0**.

Excited State	**Energy (eV)**	**Nature**	**Character of the transition**
T_1	2.60	HOMO-2→LUMO+1 (5%) **HOMO→LUMO (85%)** HOMO→LUMO+5 (3%)	CT
T_2	2.74	HOMO-2→LUMO (6%) **HOMO→LUMO+1 (84%)** HOMO→LUMO+6 (2%)	CT
T_3	2.79	**HOMO → LUMO+4 (93%)**	LE (ICz)
S1 (f=0.69)	2.81	**HOMO → LUMO (97%)**	CT

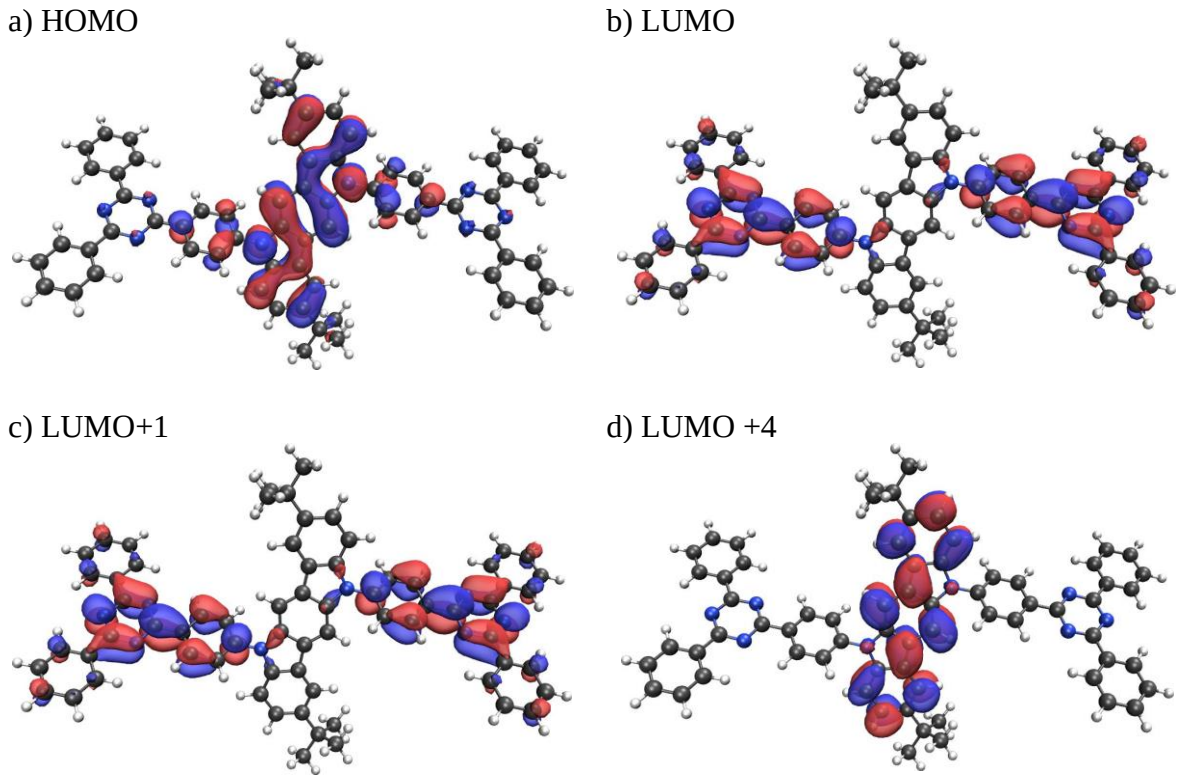

Figure S5. Electronic density surfaces of **d^{t}Bu-ICzTRZ-0**. a) HOMO, b) LUMO, c) LUMO+1, d) LUMO +4 (Isovalue for new surfaces: MO=0.02, Density=0.0004).

Table S4. Excited-state properties of **d^{t}Bu-ICzTRZ**.

Excited State	**Energy (eV)**	**Nature**	**Character of the transition**
T_1	2.65	HOMO-2→LUMO+1 (5%) **HOMO→LUMO (83%)** HOMO→LUMO+5 (5%)	CT
T_2	2.69	HOMO-2→LUMO (6%) **HOMO→LUMO+1 (83%)** HOMO→LUMO+6 (3%)	CT
T_3	2.79	**HOMO → LUMO+4 (93%)**	LE (ICz)
S1 (f=0.74)	2.86	**HOMO → LUMO (97%)**	CT

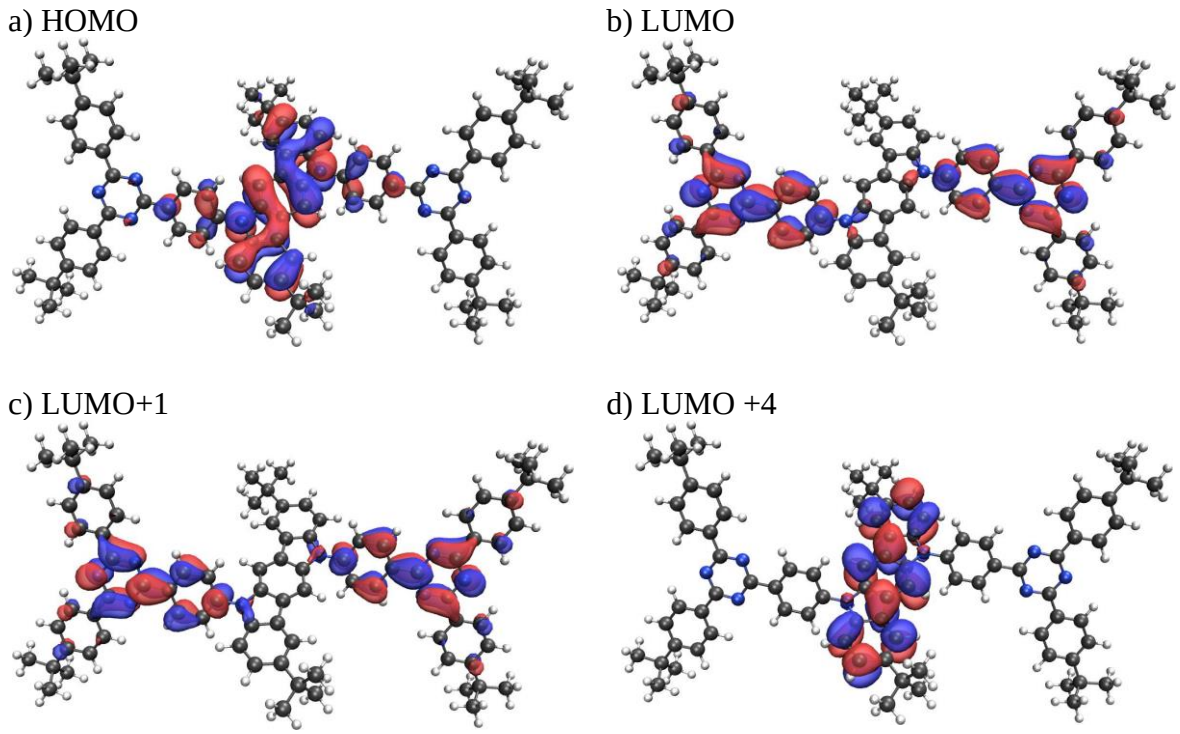

Figure S6. Electronic density surfaces of **d^{t}Bu-ICzTRZ**. a) HOMO, b) LUMO, c) LUMO+1, d) LUMO +4 (Isovalue for new surfaces: MO=0.02, Density=0.0004).

Thermal Analysis

DSC measurements of the initial **ICzTRZ** emitter were already published [20]. They show a well-resolved peak for the glass transition temperature T_g of about 253 °C. For the other three emitters, the measured DSC curves are shown below.

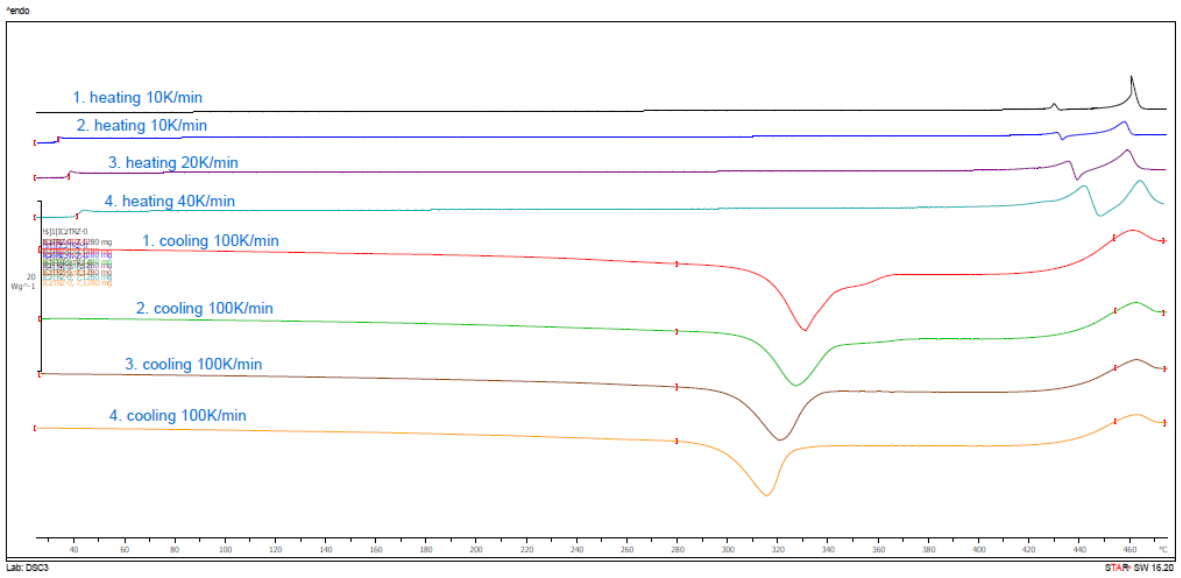

Figure S7. DSC of **ICzTRZ-0** (no T_g observed).

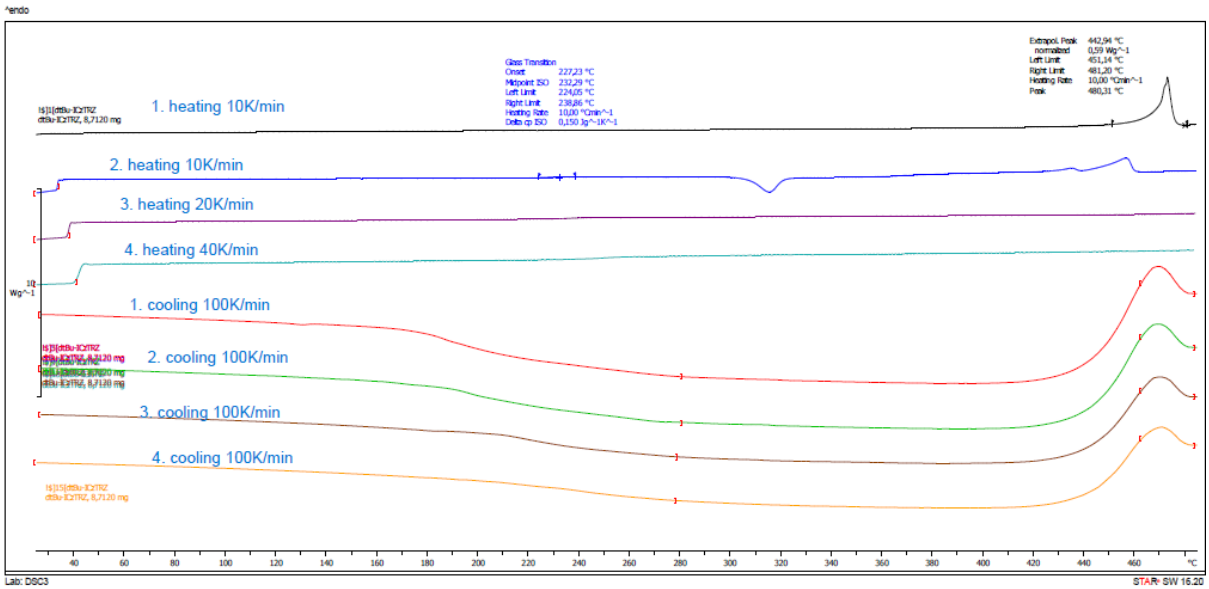

Figure S8. DSC of **d^{t}Bu-ICzTRZ-0** (T_g = 227 °C).

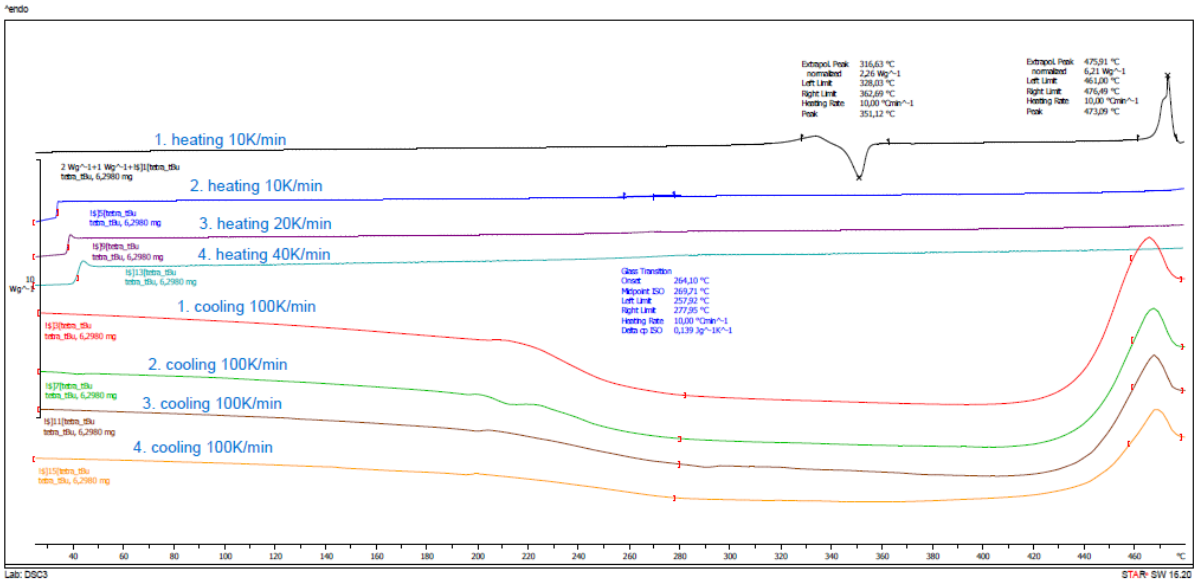

Figure S9. DSC of **d^{t}Bu-ICzTRZ** (T_g = 264 °C).

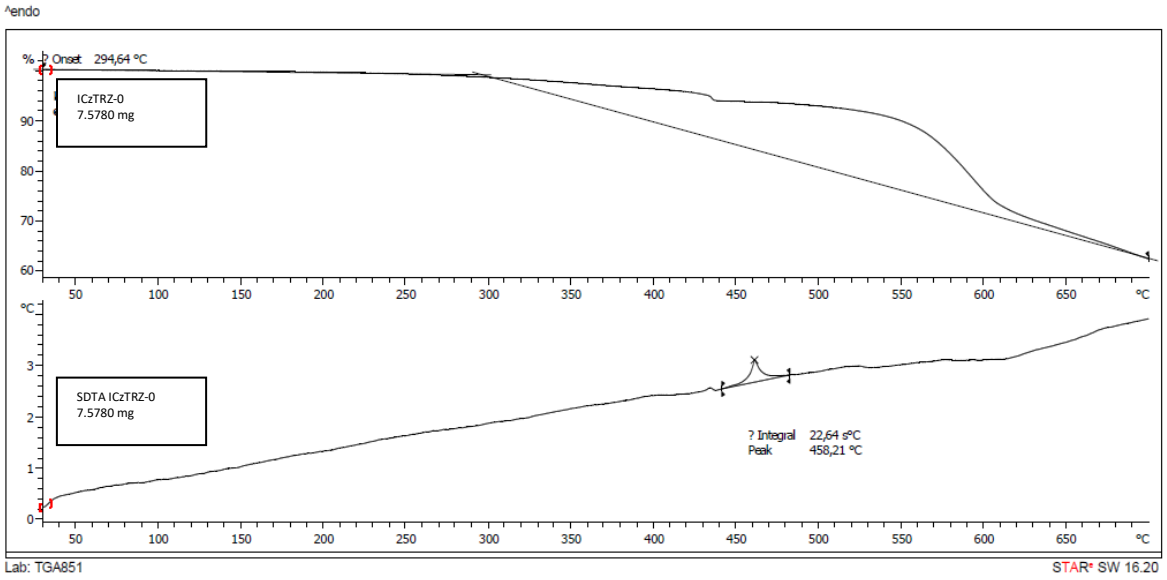

Figure S10. TGA of **ICzTRZ-0**.

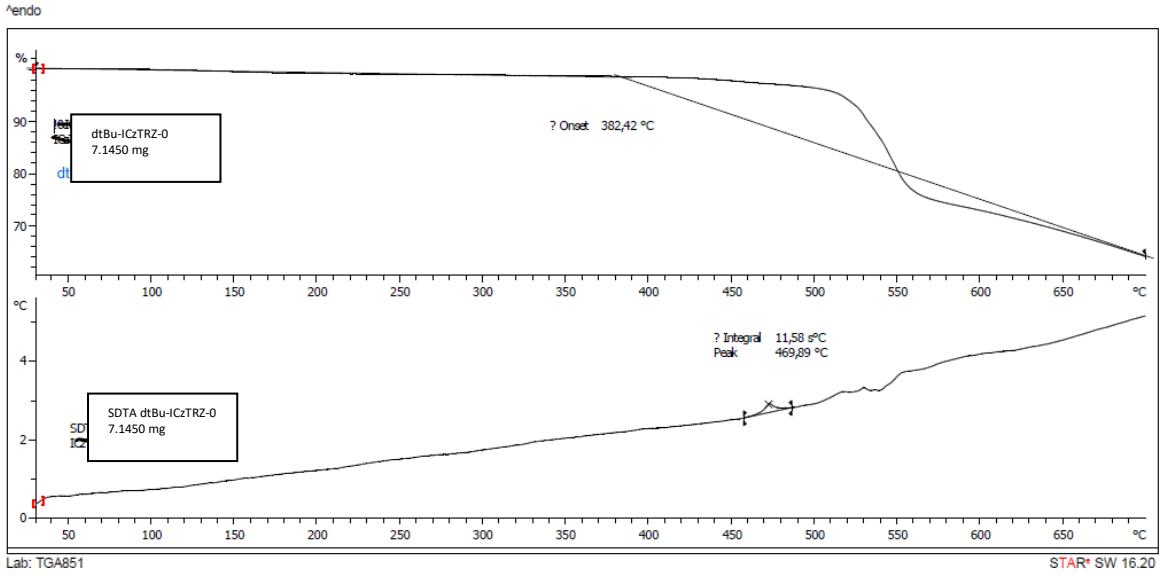

Figure S11. TGA of **d^{t}Bu-ICzTRZ-0**.

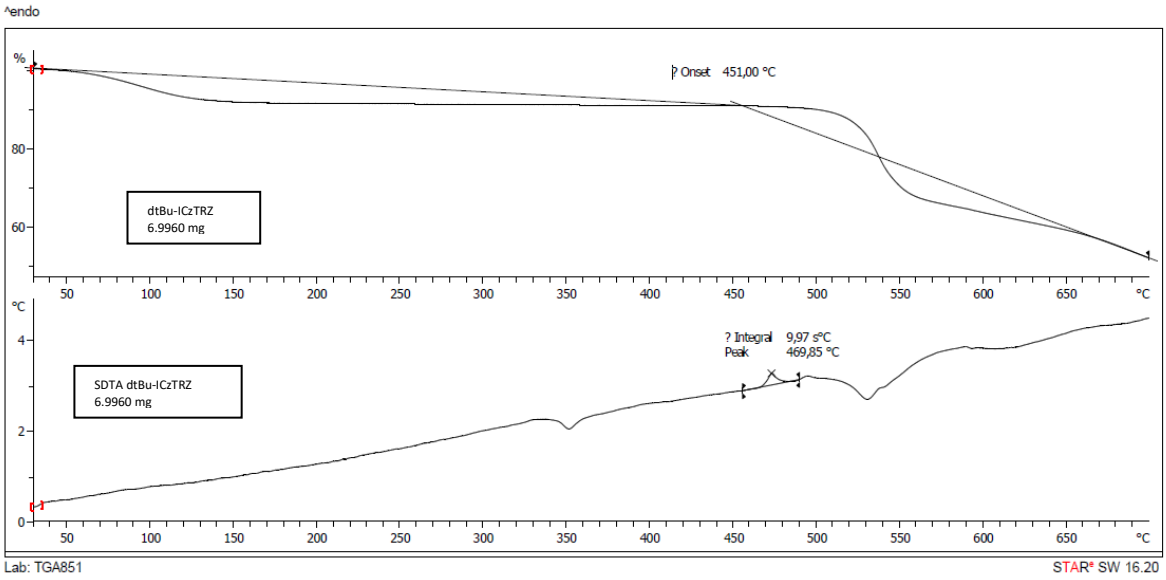

Figure S12. TGA of **d^{t}Bu-ICzTRZ**.

Molecular Geometry, Thickness and Aspect Ratio Effect

Recently, Tenopala *et al.* highlighted the factors that are correlated with controlling the orientation of TADF emitters in evaporated films *via* a thorough meta study of 230 different host/guest systems (from the combination of 130 different fluorescent and TADF emitters in neat/ doped films) results published in the literature [21].

Beside literature-reported properties, the database was populated by DFT calculated x, y, and z dimensions of the emitter, and then used to quantify their Linearity, Planarity and other related quantities. This was done since in the literature, molecules are referred to as linear or planar based on their chemical structure with no quantifiable parameter:

Linearity $L = 1 - (y/x)$

Planarity $P = 1 - (z/y)$

We followed their procedure and calculated these parameters for the four studied emitters. Furthermore, we calculated the "thickness" of the emitter molecules (z_E) as well as the ratio between the length of the emitter and the length of the host (x_E/x_H) (Table S5 & S6).

However, there is no clear correlation between these geometrical parameters and the measured orientation values of the four emitters.

Table S5. Ratio between length of emitter and host along with respective Θ values

x_E/x_H	mCP / Θ	mCBP / Θ	mCBP-CN / Θ	DPEPO / Θ
ICzTRZ	2.22 / 0.12	1.86 / 0.09	1.72 / 0.07	1.88 / 0.06
ICzTRZ-0	2.01 / 0.18	1.68 / 0.17	1.56 / 0.21	1.70 / 0.15
d^{t}Bu-ICzTRZ-0	2.01 / 0.11	1.68 / 0.09	1.56 / 0.11	1.70 / 0.09
d^{t}Bu-ICzTRZ	2.23 / 0.10	1.86 / 0.10	1.73 /0.09	1.89 / 0.09

Table S6. Calculated properties for ICz series of molecules.

Molecule	X (Å)	Y (Å)	Z (Å)	L	P	z_E
ICzTRZ	31.03	17.05	8.69	0.45	0.49	8.69
ICzTRZ-0	28.12	12.30	6.64	0.56	0.46	6.64
d^{t}Bu-ICzTRZ-0	28.11	16.62	7.56	0.41	0.55	7.56
d^{t}Bu-ICzTRZ	31.14	16.87	10.51	0.46	0.38	10.51

In addition to the inertial moments tensor of the emitter molecules (see main paper and Fig. S13 for the eigenvectors), we also calculated these values and the related aspect ratios of the host materials.

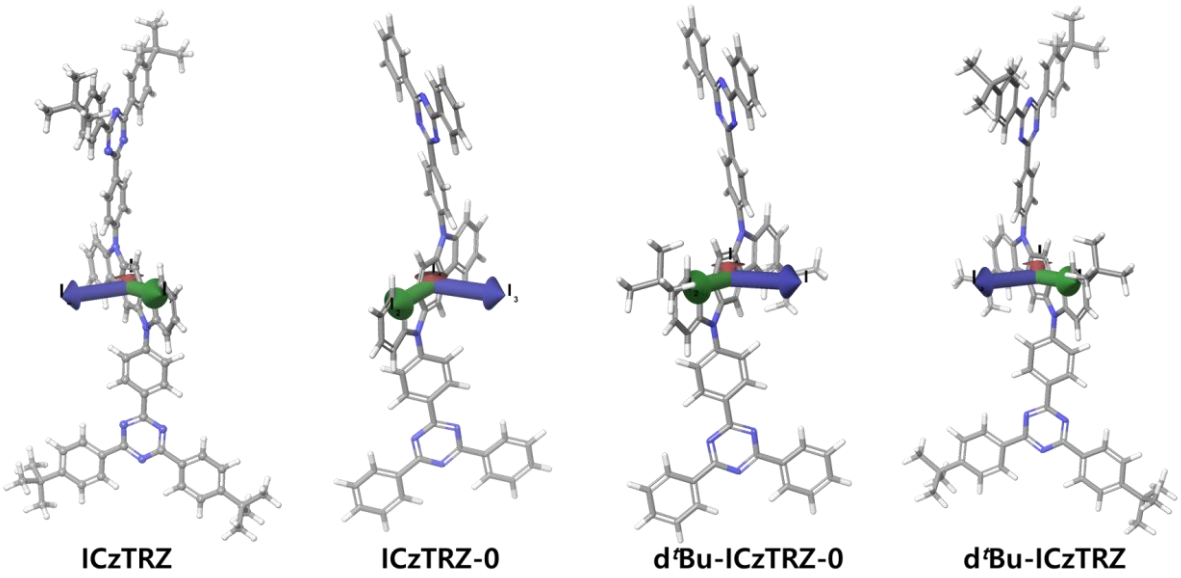

Figure S13: Inertial moment eigenvectors of the four emitters.

Table S7. Calculated aspect ratios of host molecules.

Molecule	I_1 **(amu Å²)**	I_2 **(amu Å²)**	I_3 **(amu Å²)**	**Aspect ratio** $\frac{\sqrt{I_3 \cdot I_2}}{I_1}$
mCP	1982	6632	6843	3.39
mCBP	2745	9028	11195	3.66
mCBP-CN	3526	9442	12209	3.04
DPEPO	4060	7231	7985	1.87

Orientation Measurements

The orientation factor (Θ) for emitter molecules w.r.t the host material has a significant impact on the performance of the device [19], thus has been measured in several relevant host materials and has been reported for the host mCBP-CN in the manuscript. Figures S14, S15 & S16 show the raw data for the other host materials (mCP, mCBP & DPEPO, respectively) together with fits yielding the orientation parameter Θ at the respective peak emission wavelength.

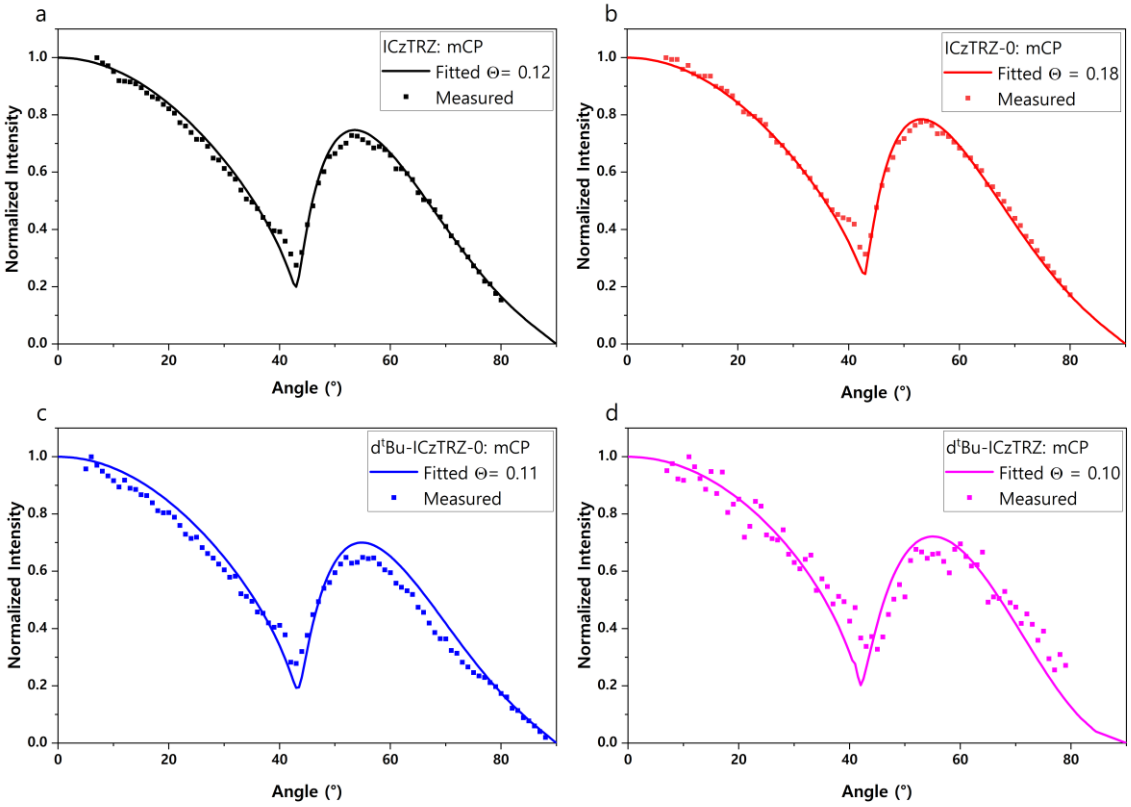

Figure S14. Orientation measurements for 10 wt% emitters in mCP.

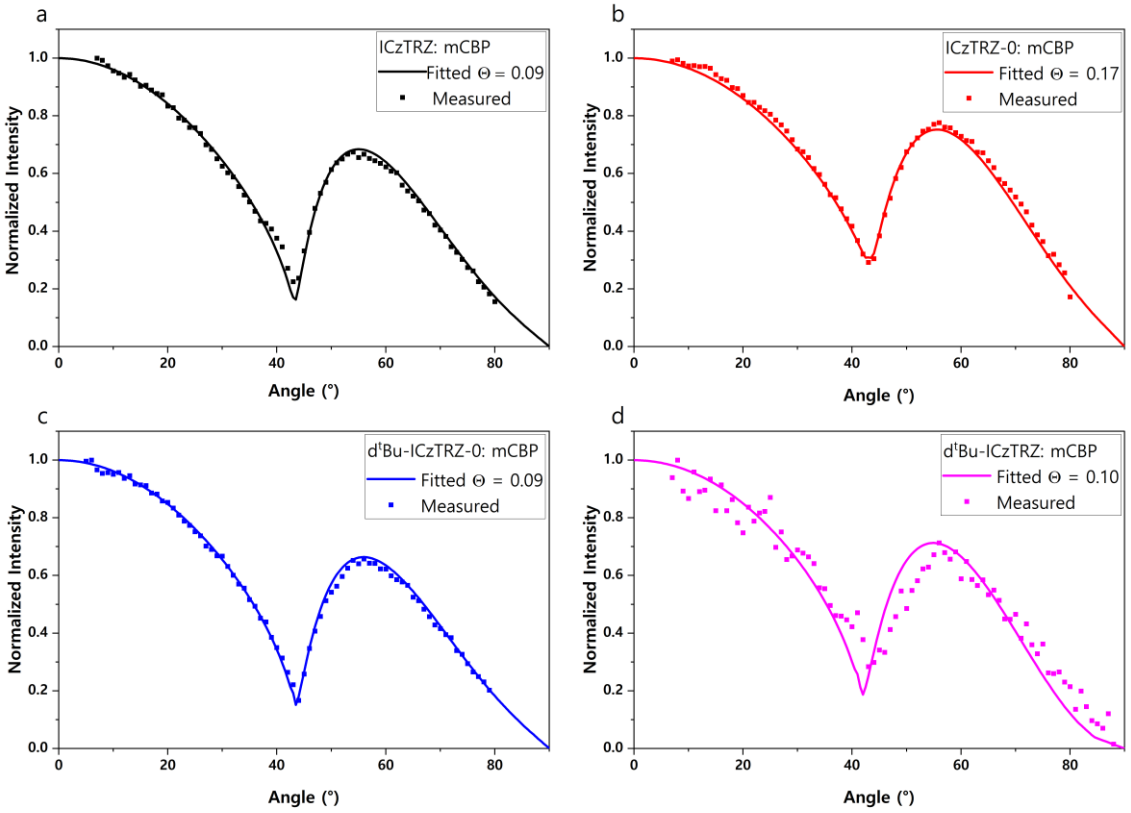

Figure S15. Orientation measurements for 10 wt% emitters in mCBP.

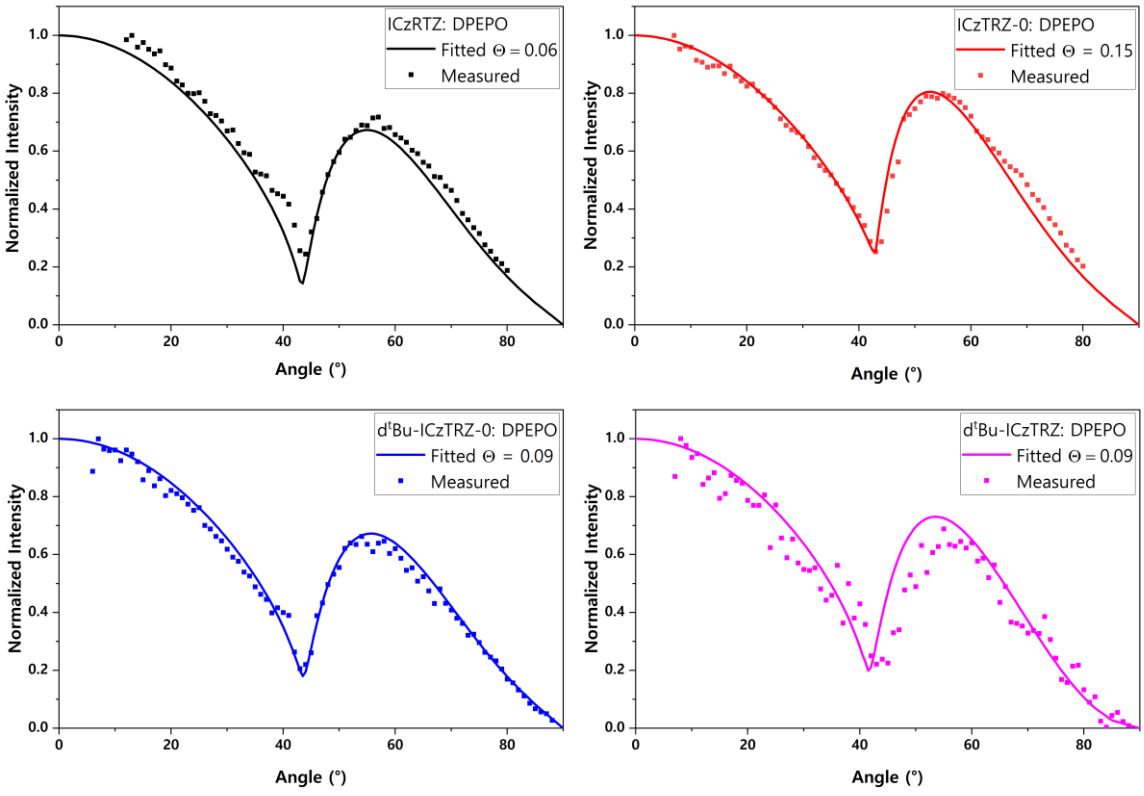

Figure S16. Orientation measurements for 10 wt% emitters in DPEPO.

OLED Device Data

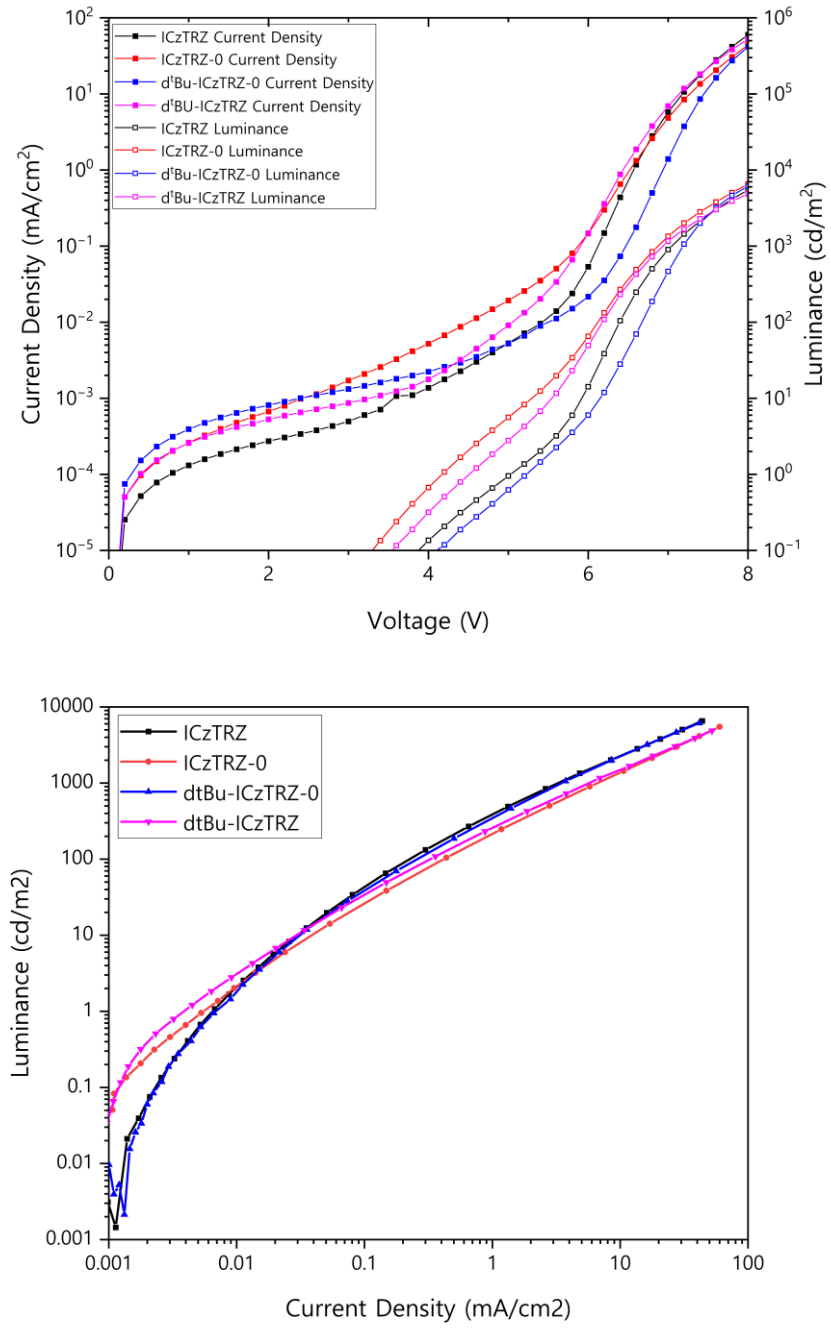

Figure S17. Comparative JVL graph (top) & Luminance vs Current Density (bottom) for the fabricated device.

Light Outcoupling Simulation

The theoretical maximum EQE for the device stack reported in the manuscript has been simulated using the commercial software SETFOS from Fluxim [5, 6]. We perform a mode analysis for the device stack while sweeping the transition dipole orientation Θ.

For our most horizontal emitter (ICzTRZ), the maximum possible outcoupled emission is about 35% with Θ = 0.07 in mCBP-CN as host, whereas for the least horizontal molecule (ICzTRZ-0), we have a value of about 28% with Θ = 0.21 in the same host matrix. Table S8 summarizes the maximum possible outcoupling emission for the series of emitters in this study in mCBP-CN host matrix.

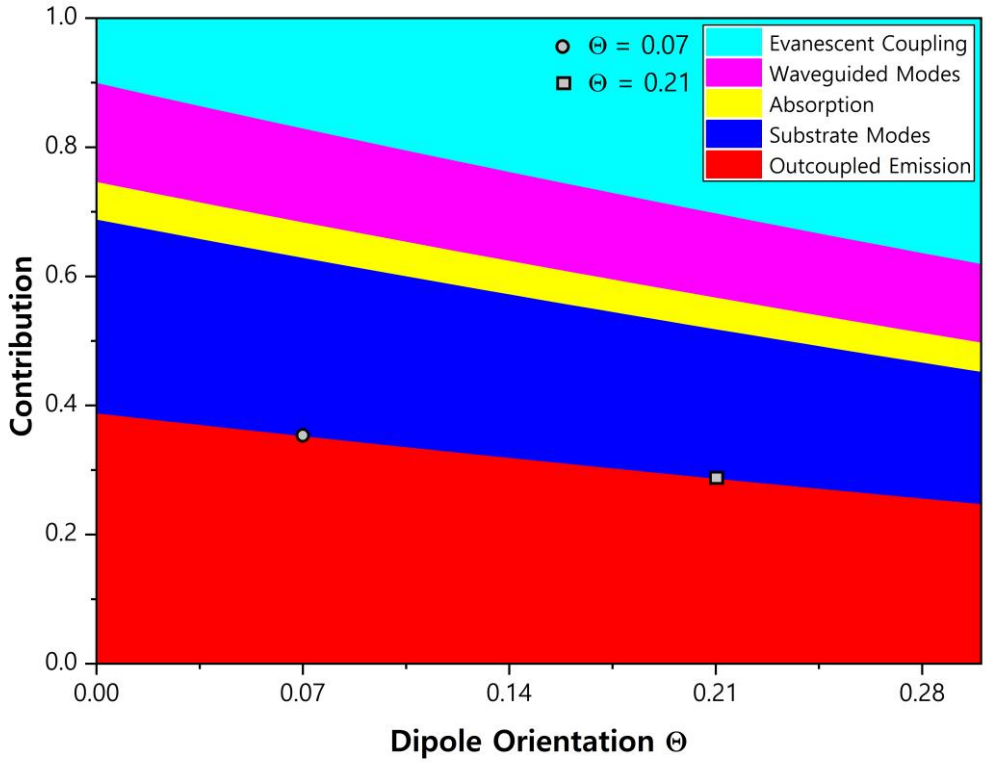

Figure S18. Simulation of the relative contributions of the different optical modes in the studied OLEDs as function of the emitter orientation.

Table S8. Simulated light outcoupling for the emitters in mCBP-CN host matrix, where also the slightly different emission spectra were considered.

Molecule	Orientation Factor	Outcoupling Factor
ICzTRZ	0.07	0.35
ICzTRZ-0	0.21	0.28
dtBu-ICzTRZ-0	0.11	0.33
dtBu-ICzTRZ	0.09	0.34

References

(1) Fluxim. *Boosting the OLED Efficiency through Fine Control over the Dipole Orientation*. https://www.fluxim.com/dipole-orientation-led.

(2) Kumar, S.; Jagielski, J.; Marcato, T.; Solari, S. F.; Shih, C.-J. Understanding the ligand effects on photophysical, optical, and electroluminescent characteristics of hybrid lead halide perovskite nanocrystal solids. *The journal of physical chemistry letters* **2019**, *10* (24), 7560-7567.

(3) Frischeisen, J.; Yokoyama, D.; Adachi, C.; Brutting, W. Determination of molecular dipole orientation in doped fluorescent organic thin films by photoluminescence measurements. *Applied Physics Letters* **2010**, *96* (7), 29. DOI: 10.1063/1.3309705.

(4) Schmidt, T. D.; Lampe, T.; Sylvinson M. R, D.; Djurovich, P. I.; Thompson, M. E.; Brütting, W. Emitter Orientation as a Key Parameter in Organic Light-Emitting Diodes. *Physical Review Applied* **2017**, *8* (3), 037001.

(5) Fluxim. *SETFOS: Simulation Software for Organic and Perovskite Solar Cells and LEDs*. https://www.fluxim.com/setfos-intro.

(6) Ruhstaller, B.; Flatz, T.; Rezzonico, D.; Moos, M.; Reinke, N.; Huber, E.; Häusermann, R.; Perucco, B. Comprehensive simulation of light-emitting and light-harvesting organic devices. In *Organic Light Emitting Materials and Devices XII*, 2008; SPIE: Vol. 7051, pp 86-97.

(7) Eli Zysman.Colman; Lee, O. S. Silico 4. DigiChemCo: St. Andrews: 2023.

(8) O'boyle, N. M.; Tenderholt, A. L.; Langner, K. M. Cclib: a library for package‐independent computational chemistry algorithms. *Journal of computational chemistry* **2008**, *29* (5), 839-845.

(9) Humphrey, W.; Dalke, A.; Schulten, K. VMD: visual molecular dynamics. *Journal of molecular graphics* **1996**, *14* (1), 33-38.

(10) Stone, J. E. An efficient library for parallel ray tracing and animation. **1998**.

(11) O'Boyle, N. Banck M. James CA Morley C. Vandermeersch T. Hutchison GR J. *Cheminform* **2011**, *3*, 1-14.

(12) O'Boyle, N. M.; Hutchison, G. R. Cinfony–combining Open Source cheminformatics toolkits behind a common interface. *Chemistry Central Journal* **2008**, *2*, 1-10.

(13) Frisch, M. J.; Trucks, G. W.; Schlegel, H. B.; Scuseria, G. E.; Robb, M. A.; Cheeseman, J. R.; Scalmani, G.; Barone, V.; Petersson, G. A.; Nakatsuji, H.; et al. Gaussian 16 Rev. C.01. Wallingford, CT, 2016.

(14) Adamo, C.; Barone, V. Toward reliable density functional methods without adjustable parameters: The PBE0 model. *The Journal of chemical physics* **1999**, *110* (13), 6158-6170.

(15) Dunning Jr, T. H. Gaussian basis sets for use in correlated molecular calculations. I. The atoms boron through neon and hydrogen. *The Journal of chemical physics* **1989**, *90* (2), 1007-1023.

(16) Hirata, S.; Head-Gordon, M. Time-dependent density functional theory within the Tamm–Dancoff approximation. *Chemical Physics Letters* **1999**, *314* (3-4), 291-299.

(17) Moral, M.; Muccioli, L.; Son, W.-J.; Olivier, Y.; Sancho-Garcia, J.-C. Theoretical rationalization of the singlet–triplet gap in OLEDs materials: Impact of charge-transfer character. *Journal of Chemical Theory and Computation* **2015**, *11* (1), 168-177.

(18) Mayr, C.; Brütting, W. Control of molecular dye orientation in organic luminescent films by the glass transition temperature of the host material. *Chemistry of Materials* **2015**, *27* (8), 2759-2762.

(19) Zhang, Z.; Crovini, E.; dos Santos, P. L.; Naqvi, B. A.; Cordes, D. B.; Slawin, A. M. Z.; Sahay, P.; Brütting, W.; Samuel, I. D. W.; Bräse, S.; et al. Efficient Sky-Blue Organic Light-Emitting Diodes Using a Highly Horizontally Oriented Thermally Activated Delayed Fluorescence Emitter. *Advanced Optical Materials* **2020**, *8* (23), 2001354.

(20) Naqvi, B. A.; Schmid, M.; Crovini, E.; Sahay, P.; Naujoks, T.; Rodella, F.; Zhang, Z.; Strohriegl, P.; Bräse, S.; Zysman-Colman, E. What controls the orientation of TADF emitters? *Frontiers in Chemistry* **2020**, *8*, 750.

(21) Tenopala-Carmona, F.; Lee, O. S.; Crovini, E.; Neferu, A. M.; Murawski, C.; Olivier, Y.; Zysman-Colman, E.; Gather, M. C. Identification of the Key Parameters for Horizontal Transition Dipole Orientation in Fluorescent and TADF Organic Light-Emitting Diodes. *Advanced Materials* **2021**, *33* (37), 2100677.